Received: 28 June 2023 | Accepted: 9 January 2024

DOI: 10.1111/jopr.13827

AMERICAN COLLEGE OF PROSTHODONTISTS
Your smile. Our specialty.®

ORIGINAL ARTICLE

Influence of exposure protocol, voxel size, and artifact removal algorithm on the trueness of segmentation utilizing an artificial-intelligence-based system

Safa Alrashed BDS, MSD[1] | **Vinicius Dutra DDS, PhD, MBA**[2] | **Tien-Min G. Chu DDS, PhD**[3] | **Chao-Chieh Yang DDS, MSD**[4,5] | **Wei-Shao Lin DDS, PhD, MBA**[4,5]

[1]Oral Biology PhD program in the College of Dentistry, Division of Restorative and Prosthetic Dentistry, The Ohio State University, Columbus, Ohio, USA

[2]Department of Oral Pathology, Medicine, and Radiology, Indiana University School of Dentistry, Indianapolis, Indiana, USA

[3]Department of Biomedical Sciences and Comprehensive Care, Indiana University School of Dentistry, Indianapolis, Indiana, USA

[4]Department of Prosthodontics, Indiana University School of Dentistry, Indianapolis, Indiana, USA

[5]Advanced Education Program in Prosthodontics, Department of Prosthodontics, Indiana University School of Dentistry, Indianapolis, Indiana, USA

Correspondence
Wei-Shao Lin, Department of Prosthodontics, Indiana University School of Dentistry, 1121 W. Michigan St, Office: DS-S313, Indianapolis, IN 46202-5186, USA.
Email: weislin@iu.edu

Abstract

Purpose: To evaluate the effects of exposure protocol, voxel sizes, and artifact removal algorithms on the trueness of segmentation in various mandible regions using an artificial intelligence (AI)-based system.

Materials and methods: Eleven dry human mandibles were scanned using a cone beam computed tomography (CBCT) scanner under differing exposure protocols (standard and ultra-low), voxel sizes (0.15 mm, 0.3 mm, and 0.45 mm), and with or without artifact removal algorithm. The resulting datasets were segmented using an AI-based system, exported as 3D models, and compared to reference files derived from a white-light laboratory scanner. Deviation measurement was performed using a computer-aided design (CAD) program and recorded as root mean square (RMS). The RMS values were used as a representation of the trueness of the AI-segmented 3D models. A 4-way ANOVA was used to assess the impact of voxel size, exposure protocol, artifact removal algorithm, and location on RMS values ($\alpha = 0.05$).

Results: Significant effects were found with voxel size ($p < 0.001$) and location ($p < 0.001$), but not with exposure protocol ($p = 0.259$) or artifact removal algorithm ($p = 0.752$). Standard exposure groups had significantly lower RMS values than the ultra-low exposure groups in the mandible body with 0.3 mm ($p = 0.014$) or 0.45 mm ($p < 0.001$) voxel sizes, the symphysis with a 0.45 mm voxel size ($p = 0.011$), and the whole mandible with a 0.45 mm voxel size ($p = 0.001$). Exposure protocol did not affect RMS values at teeth and alveolar bone ($p = 0.544$), mandible angles ($p = 0.380$), condyles ($p = 0.114$), and coronoids ($p = 0.806$) locations.

Conclusion: This study informs optimal exposure protocol and voxel size choices in CBCT imaging for true AI-based automatic segmentation with minimal radiation. The artifact removal algorithm did not influence the trueness of AI segmentation. When using an ultra-low exposure protocol to minimize patient radiation exposure in AI segmentations, a voxel size of 0.15 mm is recommended, while a voxel size of 0.45 mm should be avoided.

KEYWORDS
cone beam computed tomography, CBCT, AI segmentation, ultra-low dose

Cone beam computed tomography (CBCT) is a commonly used diagnostic tool for dental surgeries. CBCT has several advantages over conventional computed tomography (CT), including the lower radiation dose, reduced cost, short scan period, and wide availability.[1,2] On the other hand, CBCT images have less contrast resolution with more noise than conventional CT. Thus, it is more challenging to perform automatic segmentation using CBCT datasets.[3,4] Accurate segmentation is the key to achieving the desired diagnostic and planning outcomes.[5–8] Segmentation, along with the resulting 3D model, opens up a range of possibilities for various clinical applications. These include guided implant surgery, guided endodontics procedures, apical surgeries, the creation of donor teeth replicas and surgical templates for tooth autotransplantation, digital orthodontic applications, and virtual orthognathic surgery planning.[9] Traditional segmentation processes for anatomical structures have been manual, involving laborious slice-by-slice labeling, or semi-automatic, where software delineates the region of interest based on user-defined thresholds or inputs. However, these common methods, including thresholding and semi-automatic techniques, are fraught with limitations such as missing intricate bony details, being time-consuming, having a steep learning curve, observer variability, and necessitating manual adjustments. These issues are exacerbated when dealing with metal artifacts, as they require extensive manual post-processing due to similar grey values between bone and artifacts.[10] Additionally, fully automated tooth and bone segmentation that depends solely on the intensity variations in CBCT imaging is challenging due to the absence of Hounsfield units, minimal contrast differences among dental structures, and artifacts in the jaw bone area.[3,4,9]

The artificial intelligence (AI)-based segmentation showed promising performance in eliminating operator dependency.[11] A significant part of developing and integrating these AI-based automatic segmentation systems is ensuring their simplicity of use along with an accurate and fast performance that surpasses the healthcare professionals' skills and expectations.[12–15] The most common techniques used for automatic segmentation are Statistical Shape Analysis and Convolutional neural networks (CNNs).[16] In particular, CNNs use supervised learning to generate a connecting pattern of neurons compared to the architecture of the visual cortex.[13,17] CNNs showed satisfactory discriminatory intelligence in multiple clinical tasks, such as diagnosing different types of odontogenic cystic lesions, peri-apical pathosis, and alveolar bone loss.[6,18–21] Given the shortcomings of traditional segmentation methods, the recent use of CNNs has shown superior performance in modeling the dentomaxillofacial region, surpassing previous algorithms. These CNNs have demonstrated effective and promising outcomes in CBCT-based automated segmentation tasks, including the teeth, upper airway, inferior alveolar nerve canal, and maxillary sinus.[10] The U-Net architecture, renowned for automatic segmentation, adapts the CNN framework into an encoder-decoder network for efficient feature extraction and pixel-level classification, similar to SegNet's end-to-end capabilities.[22] Diagnocat (DGNCT LLC, Miami, FL) is an online platform leveraging CNNs, specifically a modified 3D U-Net architecture for semantic segmentation. Users can upload 2D or 3D digital imaging datasets for analysis, where the system generates segmentation masks for teeth, caries lesions, and anatomical structures. The architecture has two main paths: an encoder, which compresses input into abstract features, and a decoder, which expands these features to localize regions of interest accurately. The encoder reduces feature map resolution using 3D convolutions, while the decoder uses a combination of convolutions to refine and concatenate features across levels. Segmentation layers at various levels contribute to the final output through element-wise summation, enhancing the localization accuracy.[18,19,23–25]

When considering virtual planning that involves the development of segmented 3D models, CBCT imaging quality is critical.[26] The CBCT imaging quality varies depending on the scanner device, exposure parameters, and the presence of artifacts.[27,28] The resulting resolution is also influenced by the voxel size in which the smaller the voxel size, the higher the spatial resolution image. However, reducing the voxel size requires a higher radiation dose and leads to more image noise and longer scanning time.[27,29–32] Different artifacts might also appear in reconstructed 3D images. CBCT artifacts can be classified as X-ray beam-related artifacts, patient-related artifacts, scanner-related artifacts, and image noise.[33,34] CBCT image quality is negatively affected by artifacts, which then impairs the diagnosis and planning process.[35,36] Therefore, the artifact removal algorithm was developed by several CBCT manufacturers to reduce image noise, metal, and motion-related artifacts.[1,37,38] Radiation dose varies significantly among different CBCT scanners and it is highly dependent on the exposure parameters selected. The ALARA principle (as low as reasonably achievable) aims to reduce radiation dose while maintaining the necessary image quality for a specific diagnostic task. Recently an ultra-low dose algorithm was introduced, reducing the radiation dose while maintaining diagnostically acceptable image quality. The algorithm reduces the radiation dose significantly of the standard protocol.[39,40]

These CBCT-related exposure parameters and artifact removal algorithms might influence the AI-based automatic segmentation accuracy, and studies related to the accuracy of newly developed AI-based automatic segmentation platforms are scarce. Therefore, this study aimed to evaluate the effects of exposure protocol (normal and ultra-low exposure protocols), voxel sizes (0.15 mm, 0.3 mm, and 0.45 mm), and artifact removal algorithm, on the trueness of segmentation at different regions of the mandible using an established AI-based automatic segmentation system (Diagnocat AI; DGNCT LLC). The null hypotheses of this study were that the voxel sizes, artifact removal algorithm, locations in the mandible, and exposure protocol would not affect the trueness of AI segmented 3D models.

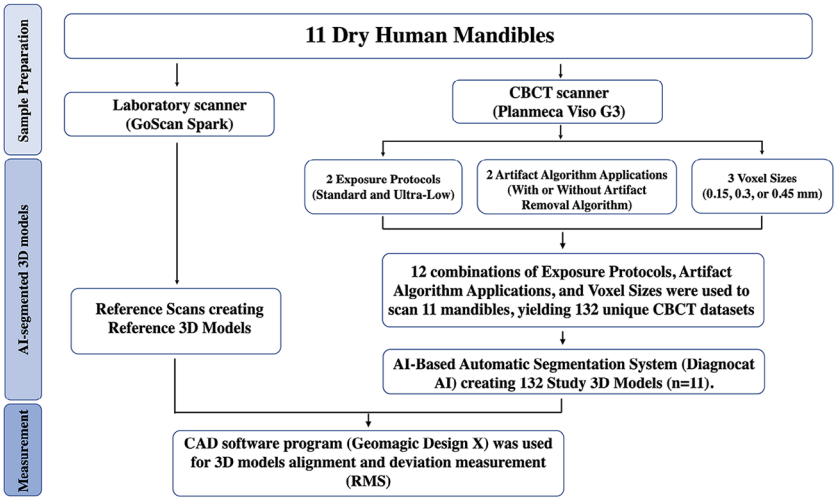

FIGURE 1 Flowchart of the study design.

MATERIAL AND METHODS

Eleven deidentified dry human mandibles were obtained from the Department of Anatomy, Cell Biology, and Physiology of Indiana University School of Medicine. The inclusion criteria for the present study were partially edentulous human mandibular jaws with at least one remaining tooth. This is due to the limitation of the AI-based automatic segmentation system (Diagnocat AI; DGNCT LLC) requiring at least one remaining tooth to process the CBCT dataset. On the other hand, mandibular jaws with any type of defect (such as fractures or tumors) were excluded. The study design and flow diagram are depicted in Figure 1.

The 11 human mandibles were scanned using a CBCT scanner (Planmeca Viso G7; Planmeca USA Inc, Hoffman Estates, IL) in a field of view (FOV) measuring 100 × 140 mm with standard exposure protocols and various voxel sizes. The first exposure protocol was set as follows: 0.15 mm voxel size, anode voltage of 100 kV, and anode current per second of 63 mAs. The second exposure protocol was set at 0.3 mm voxel size, anode voltage of 100 kV, and anode current per second of 40 mAs. The third exposure protocol was set at 0.45 mm voxel size, anode voltage of 100 kV, and anode current per second of 32 mAs. A total of 33 CBCT scans resulted and were saved as digital imaging and communications in medicine (DICOM) files (Group 1, Group 2, and Group 3, $n = 11$). Table 1 depicts the conditions of each study group. Another 33 CBCT scans were taken in the same previously mentioned exposure protocols with the application of an artifact removal algorithm. This created an additional 33 DICOM datasets (Group 4, Group 5, and Group 6, $n = 11$). All 66 DICOM datasets were segmented with an AI-based automatic segmentation system (Diagnocat AI). The resulting 3D models were saved as standard tessellation language (STL) files. In this study, patient-related artifacts were not expected to occur since the scans were performed on dry mandibles. However, the X-ray beam, scanner-related artifacts, and image noise were inspected in the scans.

The 11 human mandibles were scanned again using the same CBCT scanner (Planmeca Viso G7) with ultra-low exposure protocol in an FOV measuring 100 × 140 mm and with different voxel sizes. The first exposure protocol was set as follows: 0.15 mm voxel size, anode voltage of 100 kV, and anode current per second of 16 mAs. The second exposure protocol was set at 0.3 mm voxel size, anode voltage of 100 kV, and anode current per second of 10 mAs. The third exposure protocol was set at 0.45 mm voxel size, anode voltage of 100 kV, and anode current per second of 8 mAs. A total of 33 CBCT scans were saved as 33 DICOM datasets (Group 7, Group 8, and Group 9, $n = 11$). Similarly, another 33 CBCT scans were taken in the same ultra-low exposure protocols by applying an artifact removal algorithm. The resulting 33 DICOM datasets represent Group 10, Group 11, and Group 12 ($n = 11$). These 66 DICOM datasets were segmented by the same AI-based automatic segmentation system (Diagnocat AI; DGNCT LLC), and the resulting 3D models were saved as STL files.

Surface scans for the 11 mandibles were obtained by a white-light laboratory scanner (GoScan Spark; Creaform 3D, Canada).[41] As per the manufacturer's specifications, the scanner is capable of measuring with precision up to 0.05 mm and achieving a volumetric accuracy of 0.050 mm + 0.150 mm/m. The resulting STL files from the surface scans were used as the gold standard (reference scan) during the registration process to compare the trueness of the experiential 3D models. Each mandible's surface scan STL file was imported into CAD-CAM software (Autodesk Meshmixer; Autodesk Inc, San Francisco, CA). Anatomical areas of the mandible were selected and separated as follows: right and left condyles, right and left coronoids, right and left ramus, right and left angle of the mandible, the body of the mandible, teeth and alveolar bone, and symphysis (Figure 2). Then, each anatomical area was saved as an STL file and used as the reference for subsequent study group comparisons.

A CAD software program (Geomagic Design X; 3D Systems Inc, Rock Hill, SC) was used for 3D model alignment and deviation measurement. For each comparison, the STL

TABLE 1 Study group allocations.

Group	Exposure protocol		Artifact removal algorithm		Voxel sizes		
	Standard	Ultra-Low	No	Yes	0.15	0.3	0.45
1	√		√		√		
2	√		√			√	
3	√		√				√
4	√			√	√		
5	√			√		√	
6	√			√			√
7		√	√		√		
8		√	√			√	
9		√	√				√
10		√		√	√		
11		√		√		√	
12		√		√			√

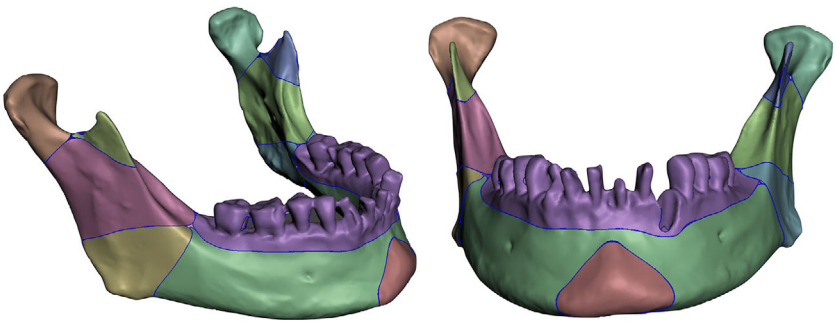

FIGURE 2 The anatomical areas, including right and left condyles, right and left coronoids, right and left ramus, right and left angle of the mandible, the body of the mandible, teeth and alveolar bone, and symphysis, were saved as individual STL files and used as the references for subsequent study group comparisons.

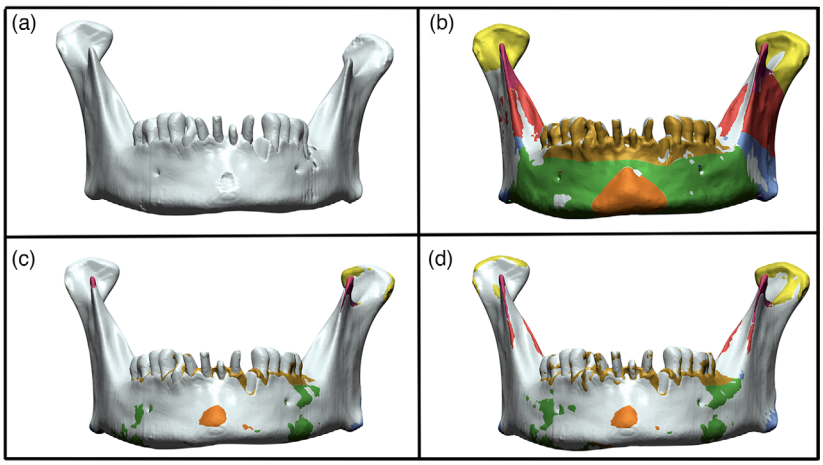

FIGURE 3 (a) STL file of the surface scan was used as a reference, and the AI-segmented 3D model was used as testing data in a CAD software program (Geomagic Design X; 3D Systems Inc, Rock Hill, SC); (b) Four anatomical points (right and left mental foramen, and right and left antegonial notch) were used for the initial alignment; (c) Initial alignment; (d) Global and fine alignment was applied to complete alignment process.

file of the surface scan was used as a reference, and the AI-segmented 3D model was used as testing data (Figure 3a). The data alignment was done using picked points, global, and fine alignments. Four anatomical points (right and left mental foramen, and right and left antegonial notch) were used for the first step in the alignment process (Figure 3b,c). Then, global and fine alignment was applied (Figure 3d). The deviation between reference surface scans and AI-segmented 3D models was evaluated by root-mean-square (RMS) values. The RMS value was recorded for each anatomical area of each mandible and the whole mandible. The RMS values were used as a representation of the trueness of the AI-segmented 3D models. Beyond the RMS values, color maps were employed to depict the differences between the AI-segmented 3D models and the matching reference surface scans. Areas where AI-segmented 3D models exceeded the size of the corresponding reference files were classified as positive deviations, represented by shades ranging

from yellow to red. Conversely, blue areas indicated negative deviations, signifying instances where the AI-segmented 3D models were smaller than the associated reference files.

With a sample size of 11 mandibles, the study had 80% power to detect an effect size of 1.0 (a 1 standard deviation difference) for differences between groups and for significance from zero deviation within groups, based on paired t-test/one sample t-test calculations and a two-sided 5% significance level. Eleven mandibles met the inclusion criteria and were included in this study. The effects of voxel size, exposure protocol, artifact removal algorithm, and location on RMS values were evaluated using a 4-way analysis of variance (ANOVA). The ANOVA model incorporated fixed effects for 4 factors, encompassing all possible interactions up to the 4-way level. It allowed for heteroscedasticity by permitting different variances for each location. The ANOVA also included random effects to address the within-mandible correlation of measurements. This model handled the repeated measures on each mandible, the correlation within each group defined by the combination of exposure protocol, artifact removal algorithm, voxel size, and the correlation among measurements at each location within a mandible. A two-sided 5% significance level was used for all tests in a software program (SAS version 9.4; SAS Institute Inc, Cary, NC).

RESULTS

The descriptive statistics are presented in Table 2. A 4-way ANOVA revealed that there was not a statistically significant 4-way interaction among the effects of voxel size, exposure protocol, artifact removal algorithm, and location ($p = 0.980$). The 3-way interaction among the effects of voxel size, exposure protocol, and location was significant ($p = 0.016$). The 2-way interactions between the effects of exposure protocol and location ($p < 0.001$), and voxel size and location ($p < 0.001$) were also significant. The effects of voxel size ($p < 0.001$) and location ($p < 0.001$) were significant, however, those of exposure protocol ($p = 0.259$) and artifact removal algorithm ($p = 0.752$) were not.

Standard exposure groups had significantly lower RMS values than those of the ultra-low exposure groups for the body of the mandible with 0.3 mm ($p = 0.014$) or 0.45 mm ($p < 0.001$) voxel sizes, for symphysis with a 0.45 mm voxel size ($p = 0.011$), and whole mandible with a 0.45 mm voxel size ($p = 0.001$). Standard exposure had significantly higher RMS values than those from the ultra-low exposure groups for ramus with a 0.45 mm voxel size ($p = 0.042$). Exposure protocol did not affect RMS values at the locations of teeth and alveolar bone ($p = 0.544$), right and left angle of the mandible ($p = 0.380$), right and left condyles ($p = 0.114$), and right and left coronoids ($p = 0.806$).

Voxel size had a significant effect for all locations, but the effect varied across locations. For right and left condyles, right and left coronoids, right and left ramus, teeth and alveolar bone, symphysis, and whole mandible, 0.45 mm voxel size groups had significantly higher RMS values than the 0.15 mm and 0.3 mm voxel sizes groups ($p < 0.001$). At the body of the mandible with standard exposure protocol, the RMS value was significantly higher in the 0.15 mm voxel size groups when compared to 0.3 mm ($p = 0.039$) and 0.45 mm ($p < 0.001$) voxel size groups. At the right and left coronoids, the RMS value was significantly higher in the 0.30 mm voxel size groups when compared to 0.15 mm voxel size groups ($p = 0.022$). For the right and left angles of the mandible and whole mandible regardless of the exposure protocol, the RMS value was significantly higher in the 0.15 mm voxel size groups when compared to 0.3 mm voxel size groups ($p = 0.017$ and $p = 0.046$, respectively).

Color maps of the surface matching differences for each group are shown in Figure 4. The green-colored area represents surface matching within a range of ± 0.1 mm. The AI-based automatic segmentation exhibits positive deviation when compared to the gold standard surface scan, depicted by the colors yellow and red. Conversely, the negative deviation is represented by the color blue. In the case of a voxel size of 0.15 mm, the mandible displays green and yellow regions (positive deviation), except for the ramus and condyle regions that appear blue (negative deviation) (Figure 4a,d,g,j). For a voxel size of 0.3 mm, positive deviation is observed at the anterior of the mandible, excluding the symphysis. Conversely, a negative deviation is present in the posterior regions (Figure 4b,e,h,k). For the 0.45 mm voxel size group, the body and symphysis areas are depicted in blue (negative deviation) (Figure 4c,f,i,l).

DISCUSSION

The null hypotheses of this study were partially rejected. Although exposure protocol and artifact removal algorithm did not affect the trueness of AI-segmented 3D models, voxel sizes and locations in the mandible demonstrated significant effects. CBCT scanners most often have a variety of scanning protocols that allow the selection of desired exposure protocols. The quality of CBCT images acquired from ultra-low exposure protocol was assessed in previous studies for different diagnostic tasks and contradicting results were found. Yeung et al. aimed to determine whether or not observers gave significantly different ratings to the CBCT image quality acquired pre- and post-root canal treatment with different exposure protocols; ultra-low dose (ULD), standard (SM), and high-resolution mode (HR). The ULD does not appear to have a negative impact on the diagnostic quality of the CBCT images based on the observers' ratings. On the other hand, observer specialty, treatment phase, type of post, and tooth number, showed significant effects.[42] Another study investigated the influence of 3 different ultra-low exposure protocols (UL-Low dose, UL-Mid Dose, and UL-High dose) on the quality of CBCT images for implant treatment planning radiographic evaluations.[39] The tube current-exposure time and the voxel size were as follows; UL-LD of 7.5mAs/400 μm, UL-MD of 22.4mAs/200 μm, and UL-HD of 28mAs/150

TABLE 2 The descriptive statistics of the root mean square (RMS, mm) of each group, mean (standard deviation).

Location	Exposure protocol	Artifact removal algorithm	Voxel size		
			0.15	0.3	0.45
Right and left angle of the mandible	Standard	No	1.127 (0.271)	1.020 (0.239)	1.116 (0.204)
	Standard	Yes	1.124 (0.276)	1.082 (0.227)	1.059 (0.282)
	Ultra-Low	No	1.111 (0.247)	0.997 (0.226)	1.104 (0.219)
	Ultra-Low	Yes	1.067 (0.229)	1.015 (0.199)	1.075 (0.241)
Teeth and alveolar bone	Standard	No	1.338 (0.057)	1.357 (0.075)	1.455 (0.137)
	Standard	Yes	1.335 (0.078)	1.379 (0.115)	1.423 (0.100)
	Ultra-Low	No	1.369 (0.065)	1.367 (0.055)	1.428 (0.077)
	Ultra-Low	Yes	1.343 (0.064)	1.360 (0.050)	1.460 (0.120)
Body of the mandible	Standard	No	1.393 (0.230)	1.336 (0.172)	1.299 (0.234)
	Standard	Yes	1.390 (0.229)	1.345 (0.199)	1.290 (0.233)
	Ultra-Low	No	1.432 (0.258)	1.408 (0.186)	1.400 (0.264)
	Ultra-Low	Yes	1.445 (0.229)	1.395 (0.198)	1.436 (0.270)
Right and left condyles	Standard	No	0.738 (0.464)	0.843 (0.519)	1.424 (0.723)
	Standard	Yes	0.787 (0.500)	0.784 (0.501)	1.270 (0.546)
	Ultra-Low	No	0.782 (0.492)	0.723 (0.368)	1.179 (0.366)
	Ultra-Low	Yes	0.766 (0.468)	0.706 (0.387)	1.328 (0.472)
Right and left coronoids	Standard	No	0.611 (0.189)	0.691 (0.182)	0.956 (0.233)
	Standard	Yes	0.590 (0.223)	0.649 (0.207)	0.976 (0.324)
	Ultra-Low	No	0.575 (0.214)	0.642 (0.188)	0.948 (0.414)
	Ultra-Low	Yes	0.569 (0.221)	0.666 (0.199)	1.039 (0.410)
Right and left ramus	Standard	No	0.732 (0.131)	0.737 (0.128)	0.843 (0.151)
	Standard	Yes	0.729 (0.131)	0.722 (0.142)	0.827 (0.163)
	Ultra-Low	No	0.750 (0.131)	0.727 (0.143)	0.771 (0.152)
	Ultra-Low	Yes	0.704 (0.159)	0.732 (0.135)	0.802 (0.159)
Symphysis	Standard	No	0.500 (0.490)	0.442 (0.523)	1.387 (0.908)
	Standard	Yes	0.496 (0.533)	0.354 (0.282)	1.527 (1.043)
	Ultra-Low	No	0.395 (0.411)	0.465 (0.492)	1.770 (0.983)
	Ultra-Low	Yes	0.494 (0.548)	0.478 (0.460)	1.938 (1.090)
Whole mandible	Standard	No	1.139 (0.120)	1.124 (0.089)	1.244 (0.151)
	Standard	Yes	1.160 (0.131)	1.141 (0.134)	1.218 (0.118)
	Ultra-Low	No	1.198 (0.137)	1.150 (0.091)	1.272 (0.154)
	Ultra-Low	Yes	1.185 (0.140)	1.149 (0.106)	1.317 (0.162)

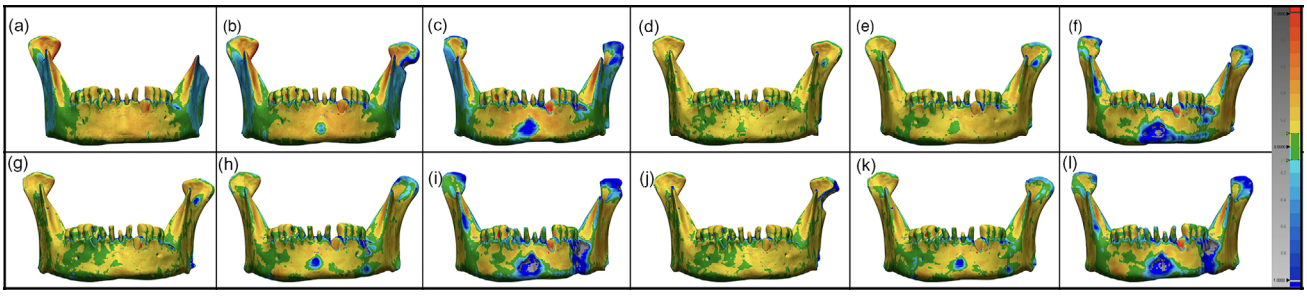

FIGURE 4 Color map alignment deviation between gold standard surface scan and AI-based automatic segmentation STL files for each group. Red color depicts as positive deviation of +1.00 mm, green color depicts the deviation between +0.10 mm to −0.10 mm, and blue color depicts negative deviation of −1.00 mm. (a) Group 1; (b) Group 2; (c) Group 3; (d) Group 4; (e) Group 5; (f) Group 6; (g) Group 7; (h) Group 8; (i) Group 9; (j) Group 10; (k) Group 11; (l) Group 12.

μm. The UL-Low dose exposure protocol produced CBCT images that were not of acceptable diagnostic quality for implant site evaluation. However, UL-Mid Dose and UL-High dose exposure protocols produced CBCT images that were of acceptable diagnostic quality in terms of image quality, visualization of anatomical structures, and bone quality evaluation. In some circumstances, a standard exposure protocol may be required to distinguish the borders of the maxillary sinus and mandibular canal.[39]

Based on the present study results and the previous study findings,[39] due to the limitation of AI-based automatic segmentation at the body of mandible, symphysis, and overall whole mandible, it is not recommended to use AI-based automatic segmentation for implant planning or orthognathic surgery with ultra-low exposure protocol along with 0.45 mm voxel size.[43] Implant planning or orthognathic surgery requires accurate segmentation from CBCT scans to ensure the proper fit of surgical templates. In contrast, ultra-low exposure protocol was recommended to evaluate maxillary impacted canines.[44] In the medical field, physicians explored the use of ultra-low-dose CBCT scans as a means of reducing radiation exposure in patients undergoing ear surgery. The study concluded that the use of ultra-low-dose CBCT scans provided clinically sufficient image quality of the ear, making it a viable option.[45] According to the findings of a medical retrospective cohort study, the diagnosis accuracy of ultra-low-dose CBCT scans for radiographically occult extremities fractures (82.8%) is somewhat lower than the diagnostic accuracy of standard CBCT. The amount of radiation exposure, on the other hand, was lowered by a factor of seven, from 10.7 Sv to 1.5 Sv.[40]

Another key finding in the present study was that exposure protocol did not affect the AI-based automatic segmentation trueness of all anatomical areas when the scans were taken with a 0.15 mm voxel size. This might be because the small voxel size produced high-resolution scans that were not affected by the noise from the ultra-low exposure protocol. Considering these findings, the utilization of an ultra-low exposure protocol is proposed when the chosen voxel size is 0.15 mm. This recommendation stems from the professional obligation of dental practitioners to mitigate radiation dose exposure to patients as much as practicable. With a voxel size of 0.3 mm using the ultra-low exposure protocol, the segmentation trueness was compromised at the body of the mandible, although trueness was maintained in all other anatomical locations. When increasing the voxel size to 0.45 mm, the symphysis, body, and the entirety of the mandible showed decreased segmentation trueness under ultra-low exposure protocol compared to a standard exposure. Conversely, the ramus demonstrated superior segmentation trueness under ultra-low exposure protocol compared to a standard exposure. This phenomenon suggested a promising outlook for AI-based automatic segmentation utilizing ultra-low exposure protocol. Even with the reduced radiation dose, AI is capable of producing true segmentation for these scans.

The second objective of the present study was to assess the influence of CBCT voxel size on AI-based automatic segmentation trueness. The CBCT scanner (Planmeca Viso G7) used in this study offers 5 voxel size options: 0.075, 0.15, 0.3, 0.45, and 0.6 mm. Of these, the 0.15, 0.3, and 0.45 mm voxel sizes are within the range found in most commercially available CBCT scanners. Studies utilizing these voxel sizes have been conducted to detect root fractures, root resorption, caries lesions, and TMJ erosions, measure 3D segmentations, evaluate bone volume, and assess soft tissue thickness.[31] This study aimed to use parameters that cover a wide array of clinical applications; therefore, voxel sizes of 0.15, 0.3, and 0.45 mm were selected. One study observed no significant difference in the linear measurement of bone height and thickness across CBCT images reconstructed using voxel sizes of 0.1, 0.2, 0.3, and 0.4 mm.[46] Furthermore, there appeared to be no difference in the accuracy of linear measurements on 3D reconstructed models between 0.2 and 0.4 mm voxel sizes,[47,48] as well as between 0.15 and 0.3 mm voxel sizes.[30] Similar findings were reported for the accuracy of 3D reconstructed models and the reference optical scan model at voxel sizes of 0.1, 0.2, and 0.3 mm.[49] The volumetric accuracy of 3D tooth reconstruction remained unaffected across different voxel sizes; specifically, 0.15 and 0.3 mm.[50] In contrast, a study found that the accuracy of volumetric measurements in CBCT scanning was affected by voxel sizes and Hounsfield unit thresholds.[51] For the detection of fine details, a smaller voxel size is recommended.[52] The visual analysis of bone structure is also affected by voxel size.[53] Another study reported that the influence of voxel size on accuracy may depend on the specific CBCT machine used.[54] The present study reveals that a voxel size of 0.45 mm has an adverse effect on the trueness of AI-based automatic segmentation at various anatomical regions, such as condyle, coronoids, ramus, alveolar bone, teeth, symphysis, and the entire mandible. To ensure true segmentation for implant surgical guide fabrication, it is recommended to use either 0.15 mm or 0.3 mm voxel size with the AI-based automatic segmentation technique. In addition to these findings, it is important to note that the optimal voxel size, considering the trade-off with radiation dose, is 0.3 mm.

The results of this study indicated that the artifact removal algorithm has no impact on segmentation trueness. Given the absence of metal structures in the mandible, Patient-related artifacts were not anticipated in this study because the scans were done on dry mandibles. However, the artifact removal algorithm was used to reduce the X-ray beam, scanner-related artifacts, and image noise. In line with a prior study, the use of a metal artifact reduction option led to less variation in grey values and a higher contrast-to-noise ratio. Optimal results were obtained when the algorithm was activated, and the phantom was positioned centrally within the volume. Image quality also improved with an increase in peak kilovoltage.[38] The lower RMS value observed at the condyles and symphysis area can be attributed to the object's location within the FOV. Previous research has demonstrated that objects positioned near the FOV margin tend to exhibit more noticeable halation artifacts, providing an additional explanation for the observed results.[55] However, a contention existed concerning

the effect of artifact removal algorithms on the accuracy of CBCT images in diagnosing vertical root fractures. One study reported improved visibility,[56] while another indicated the opposite effect.[57] These contrasting results could stem from variations in the CBCT machines employed in the different studies.

The AI-based automatic segmentation system (Diagnocat AI) used in this study is an established start-up platform. It offers fully automated segmentation for CBCT images and pre-diagnoses for 2D dental radiographs. This is achieved through a pipeline of multiple pre-trained CNNs and an algorithmic slice extraction process.[18,19,23–25] Several other established companies, including leading players and known start-ups, offer similar services. These include Relu (Relu BV, Leuven, Belgium), Materialise Mimics Viewer (Materialise, Leuven, Belgium), and Brainlab Elements (Brainlab AG; Munich, Germany).[16] Relu (Relu BV), an established start-up, specializes in fully automated, cloud-based segmentation for CBCT and CT images used in the cranio-maxillofacial field. It is ISO 13485 compliant, and a CE mark is pending. Materialise Mimics Viewer (Materialise) features a cloud-based viewer that facilitates online visualization and segmentation of DICOM files, with fully automatic segmentation available for a range of CBCT and CT scans. The Mimics Automatic Algorithms are FDA 510(k) approved and standalone CE-marked medical devices. Brainlab Elements (Brainlab AG) offers a comprehensive suite of applications for medical image processing, including data transfer, co-registration, segmentation, and planning. While it can automatically segment cranial and facial bones, as well as differentiate between cortical and cancellous bone, it does not provide segmentation for teeth.[16] A recent study indicated that while manual segmentation yielded the highest accuracy, automated AI-based methods from Relu, Diagnocat, Materialise, and Brainlab demonstrated very similar performance to one another. It also assessed the average segmentation times for CT and CBCT with and without artifacts. The results showed that the self-developed AI model was the fastest, averaging 2:03 (2 min and 3 s), outperforming Brainlab at 3:54 and Diagnocat at 4:52. Manual segmentation durations for experts and novices were comparable, at 26:09 and 22:54 respectively, while Materialize averaged the longest at 85:54.[16] The authors selected Diagnocat AI for this present study due to its ability to produce AI-based radiological reports and segmentations from 2D or 3D images, its comparable segmentation accuracy to other established AI platforms, and its rapid turnaround for radiological reports.

The study's primary limitation is its reliance on a solitary AI-based automatic segmentation system and the use of dry human mandibles exclusively. The chosen mandibles were meant to match surface scans that function as standard reference models; however, this method does not account for the potential impact of surrounding soft tissues or patient movement on the AI's segmentation accuracy. With only 11 dry human mandibles available, the study had a limited capacity to rigorously assess artifact influences. The limited number of metallic objects and the absence of patient motion during imaging restricted the thorough evaluation of the artifact removal algorithm's effectiveness. This limitation highlights a direction for future research to assess artifact removal in scenarios including metal restorations, implants, and live patient imaging conditions. Moreover, the study did not address the complexities of the maxilla, which could limit the applicability of the findings. Beyond the root mean square (RMS) metric, which measures surface overlap discrepancies, other metrics cited in the literature for AI segmentation accuracy, such as the dice similarity coefficient (DSC), the 95% Hausdorff distance (HD), and the intersection over union (IoU), offer additional dimensions for future evaluations of AI-based segmentation's nuance.[10] The employment of a singular CBCT machine poses another concern due to the potential for variability across different devices. Although the sample size was statistically valid, the modest number of 11 mandibles suggests the necessity for broader research to validate segmentation accuracy across diverse AI systems comprehensively. Future studies should also consider the effects of artifact removal on mandibles with metal constructs and the clinical significance of geometric accuracy in AI-segmented 3D models. While the AI-based automatic segmentation systems in commercial availability show promise, their generalizability and reliability await confirmation against an extensive external dataset. Ideally, this data would be collected from a broad patient base or compiled from multiple dental institutions.[16]

CONCLUSION

The findings in this study carry implications for the choice of exposure and voxel size in CBCT imaging, aiming to balance true AI-based automatic segmentation with minimal radiation exposure. The ultra-low exposure protocol does not impact the trueness of AI-based automatic segmentation unless scans are taken with 0.3 or 0.45 mm voxel sizes specifically at the body of the mandible and with a 0.45 mm voxel size at the symphysis area and across the entire mandible. When performing AI segmentations, the utilization of ultra-low exposure protocol is proposed when the chosen voxel size is 0.15 mm, and the voxel size of 0.45 mm should be avoided. The artifact removal algorithm was found not to influence the trueness of AI segmentation.

ACKNOWLEDGMENTS

The authors did not receive any grants from funding agencies nor were they under any contractual agreement for this research. We express our gratitude to Doug Gillespie and Diagnocat AI (DGNCT LLC, Miami, FL) for providing the AI segmentations used in this research at no cost. We also extend our thanks to Dr. Andrew S. Deane, Vice Chair for Outreach, for the invaluable support in providing mandible samples from the Department of Anatomy, Cell Biology & Physiology at the Indiana University School of Medicine. Special acknowledgment is also due to Chauncey Frend, Sr. Analyst Programmer at the UITS RT Advanced Visualization

Lab, part of Indiana University Information Technology Services, for the dedicated efforts in conducting the surface scans of the mandibles.

ORCID

Vinicius Dutra DDS, PhD, MBA https://orcid.org/0000-0002-0534-3067
Tien-Min G. Chu DDS, PhD https://orcid.org/0000-0002-7190-837X
Chao-Chieh Yang DDS, MSD https://orcid.org/0000-0002-6008-0650
Wei-Shao Lin DDS, PhD, MBA https://orcid.org/0000-0002-4881-0569

REFERENCES

1. Scarfe WC, Farman AG. What is cone-beam CT and how does it work? Dent Clin North Am 2008;52(4):707-30
2. Kamburoğlu K, Kiliç C, Ozen T, Yüksel SP. Measurements of mandibular canal region obtained by cone-beam computed tomography: a cadaveric study. Oral Surg Oral Med Oral Pathol Oral Radiol Endod 2009;107(2):e34-e42
3. Qiu B, van der Wel H, Kraeima J, Hendrik Glas H, Guo J, Borra RJH, et al. Robust and accurate mandible segmentation on dental CBCT scans affected by metal artifacts using a prior shape model. J Pers Med 2021;11(5):364
4. Loubele M, Maes F, Schutyser F, Marchal G, Jacobs R, Suetens P. Assessment of bone segmentation quality of cone-beam CT versus multislice spiral CT: a pilot study. Oral Surg Oral Med Oral Pathol Oral Radiol Endod 2006;102(2):225-34
5. Linz C, Müller-Richter UD, Buck AK, Mottok A, Ritter C, Schneider P, et al. Performance of cone beam computed tomography in comparison to conventional imaging techniques for the detection of bone invasion in oral cancer. Int J Oral Maxillofac Surg 2015;44(1):8-15
6. Lee JH, Kim DH, Jeong SN. Diagnosis of cystic lesions using panoramic and cone beam computed tomographic images based on deep learning neural network. Oral Dis 2020;26(1):152-58
7. Junqueira RB, Verner FS, Campos CN, Devito KL, do Carmo AM. Detection of vertical root fractures in the presence of intracanal metallic post: a comparison between periapical radiography and cone-beam computed tomography. J Endod 2013;39(12):1620-24
8. Zheng Z, Yan H, Setzer FC, Shi KJ, Mupparapu M, Li J. Anatomically constrained deep learning for automating dental CBCT segmentation and lesion detection. IEEE Trans Autom Sci Eng 2020;18(2):603-14
9. Lahoud P, EzEldeen M, Beznik T, Willems H, Leite A, Van Gerven A, et al. Artificial intelligence for fast and accurate 3-dimensional tooth segmentation on cone-beam computed tomography. J Endod 2021;47(5):827-35
10. Preda F, Morgan N, Van Gerven A, Nogueira-Reis F, Smolders A, Wang X, et al. Deep convolutional neural network-based automated segmentation of the maxillofacial complex from cone-beam computed tomography: a validation study. J Dent 2022;124:104238
11. Qiu B, van der Wel H, Kraeima J, Glas HH, Guo J, Borra RJH, et al. Mandible segmentation of dental CBCT scans affected by metal artifacts using coarse-to-fine learning model. J Pers Med 2021;11(6):560
12. Litjens G, Kooi T, Bejnordi BE, Setio AAA, Ciompi F, Ghafoorian M, et al. A survey on deep learning in medical image analysis. Med Image Anal 2017;42:60-88
13. Yasaka K, Akai H, Kunimatsu A, Kiryu S, Abe O. Deep learning with convolutional neural network in radiology. Jpn J Radiol 2018;36(4):257-72
14. Revilla-León M, Gómez-Polo M, Vyas S, Barmak BA, Galluci GO, Att W, et al. Artificial intelligence applications in implant dentistry: a systematic review. J Prosthet Dent 2023;129(2):293-300
15. Hung KF, Yeung AWK, Bornstein MM, Schwendicke F. Personalized dental medicine, artificial intelligence, and their relevance for dentomaxillofacial imaging. Dentomaxillofac Radiol 2023;52(1):20220335
16. Ileşan RR, Beyer M, Kunz C, Thieringer FM. Comparison of artificial intelligence-based applications for mandible segmentation: from established platforms to in-house-developed software. Bioengineering (Basel) 2023;10(5):604
17. Liu F, Gao L, Wan J, Lyu ZL, Huang YY, Liu C, et al. Recognition of digital dental X-ray images using a convolutional neural network. J Digit Imaging 2023;36(1):73-79
18. Ezhov M, Gusarev M, Golitsyna M, Yates JM, Kushnerev E, Tamimi D, et al. Clinically applicable artificial intelligence system for dental diagnosis with CBCT. Sci Rep. 2021;11(1):15006
19. Orhan K, Bayrakdar IS, Ezhov M, Kravtsov A, Özyürek T. Evaluation of artificial intelligence for detecting periapical pathosis on cone-beam computed tomography scans. Int Endod J 2020;53(5):680-89
20. Alotaibi G, Awawdeh M, Farook FF, Aljohani M, Aldhafiri RM, Aldhoayan M. Artificial intelligence (AI) diagnostic tools: utilizing a convolutional neural network (CNN) to assess periodontal bone level radiographically-a retrospective study. BMC Oral Health 2022;22(1):399
21. Kwak GH, Kwak EJ, Song JM, Park HR, Jung YH, Cho BH, et al. Automatic mandibular canal detection using a deep convolutional neural network. Sci Rep 2020;10(1):5711
22. Yeung M, Sala E, Schönlieb CB, Rundo L. Unified focal loss: generalising dice and cross entropy-based losses to handle class imbalanced medical image segmentation. Comput Med Imaging Graph 2022;95:102026
23. Kurt Bayrakdar S, Orhan K, Bayrakdar IS, Bilgir E, Ezhov M, Gusarev M, et al. A deep learning approach for dental implant planning in cone-beam computed tomography images. BMC Med Imaging 2021;21(1):86
24. Zadrożny Ł, Regulski P, Brus-Sawczuk K, Czajkowska M, Parkanyi L, Ganz S, et al. Artificial intelligence application in assessment of panoramic radiographs. Diagnostics (Basel). 2022;12(1):224
25. Amasya H, Alkhader M, Serindere G, Futyma-Gąbka K, Aktuna Belgin C, Gusarev M, et al. Evaluation of a decision support system developed with deep learning approach for detecting dental caries with cone-beam computed tomography imaging. Diagnostics (Basel) 2023;13(22):3471
26. Jacobs R. Dental cone beam CT and its justified use in oral health care. JBR-BTR 2011;94(5):254-65
27. Hassan B, Couto Souza P, Jacobs R, de Azambuja Berti S, van der Stelt P. Influence of scanning and reconstruction parameters on quality of three-dimensional surface models of the dental arches from cone beam computed tomography. Clin Oral Investig 2010;14(3):303-10
28. Kamburoğlu K, Murat S, Kolsuz E, Kurt H, Yüksel S, Paksoy C. Comparative assessment of subjective image quality of cross-sectional cone-beam computed tomography scans. J Oral Sci 2011;53(4):501-8
29. Molen AD. Considerations in the use of cone-beam computed tomography for buccal bone measurements. Am J Orthod Dentofacial Orthop 2010;137(S4):S130-35
30. Moshfeghi M, Tavakoli MA, Hosseini ET, Hosseini AT, Hosseini IT. Analysis of linear measurement accuracy obtained by cone beam computed tomography (CBCT-NewTom VG). Dent Res J (Isfahan) 2012;9(S1):S57-S62
31. Spin-Neto R, Gotfredsen E, Wenzel A. Impact of voxel size variation on CBCT-based diagnostic outcome in dentistry: a systematic review. J Digit Imaging 2013;26(4):813-20
32. Maret D, Telmon N, Peters OA, Lepage B, Treil J, Inglèse JM, et al. Effect of voxel size on the accuracy of 3D reconstructions with cone beam CT. Dentomaxillofac Radiol 2012;41(8):649-55
33. Schulze R, Heil U, Gross D, Bruellmann DD, Dranischnikow E, Schwanecke U, et al. Artefacts in CBCT: a review. Dentomaxillofac Radiol 2011;40(5):265-73
34. Nagarajappa AK, Dwivedi N, Tiwari R. Artifacts: the downturn of CBCT image. J Int Soc Prev Community Dent 2015;5(6):440-45

35. Pauwels R, Stamatakis H, Bosmans H, Bogaerts R, Jacobs R, Horner K, et al. Quantification of metal artifacts on cone beam computed tomography images. Clin Oral Implants Res 2013;24 (Suppl A100):94-99
36. Pauwels R, Araki K, Siewerdsen JH, Thongvigitmanee SS. Technical aspects of dental CBCT: state of the art. Dentomaxillofac Radiol 2015;44(1):20140224
37. Bechara B, McMahan CA, Geha H, Noujeim M. Evaluation of a cone beam CT artefact reduction algorithm. Dentomaxillofac Radiol 2012;41(5):422-28
38. Bechara BB, Moore WS, McMahan CA, Noujeim M. Metal artefact reduction with cone beam CT: an in vitro study. Dentomaxillofac Radiol 2012;41(3):248-53
39. Liljeholm R, Kadesjö N, Benchimol D, Hellén-Halme K, Shi XQ. Cone-beam computed tomography with ultra-low dose protocols for pre-implant radiographic assessment: an in vitro study. Eur J Oral Implantol 2017;10(3):351-59
40. Murphy MC, Gibney B, Walsh J, Orpen G, Kenny E, Bolster F, et al. Ultra-low-dose cone-beam CT compared to standard dose in the assessment for acute fractures. Skeletal Radiol 2022;51(1): 153-159
41. Kalinowski M, Hindmarch J, Luhmann T. Accuracy investigations of hand-held scanning systems using different dumbbell artefacts [Internet]. Available from: https://isprs-archives.copernicus.org/articles/XLIII-B2-2022/401/2022/Accessed 6/27/23
42. Yeung AWK, Harper B, Zhang C, Neelakantan P, Bornstein MM. Do different cone beam computed tomography exposure protocols influence subjective image quality prior to and after root canal treatment? Clin Oral Investig 2021;25(4):2119-27
43. Li DTS, Leung YY. Patient-specific implants in orthognathic surgery. Oral Maxillofac Surg Clin North Am 2023;35(1):61-69
44. Ihlis RL, Kadesjö N, Tsilingaridis G, Benchimol D, Shi XQ. Image quality assessment of low-dose protocols in cone beam computed tomography of the anterior maxilla. Oral Surg Oral Med Oral Pathol Oral Radiol 2022;133(4):483-91
45. Tamminen P, Järnstedt J, Lehtinen A, Numminen J, Lehtimäki L, Rautiainen M, et al. Ultra-low-dose CBCT scan: rational map for ear surgery. Eur Arch Otorhinolaryngol 2023;280(3):1161-68
46. Kehrwald R, Castro HS, Salmeron S, Matheus RA, Santaella GM, Queiroz PM. Influence of voxel size on CBCT images for dental implants planning. Eur J Dent 2022;16(2):381-85
47. Mukhia N, Birur NP, Shubhasini AR, Shubha G, Keerthi G. Dimensional measurement accuracy of 3-dimensional models from cone beam computed tomography using different voxel sizes. Oral Surg Oral Med Oral Pathol Oral Radiol 2021;132(3):361-69
48. Fernandes TM, Adamczyk J, Poleti ML, Henriques JF, Friedland B, Garib DG. Comparison between 3D volumetric rendering and multiplanar slices on the reliability of linear measurements on CBCT images: an in vitro study. J Appl Oral Sci 2015;23(1):56-63
49. Mai HN, Lee DH. Effects of exposure parameters and voxel size for cone-beam computed tomography on the image matching accuracy with an optical dental scan image: an in vitro study. Biomed Res Int 2021;2021:6971828
50. Sang YH, Hu HC, Lu SH, Wu YW, Li WR, Tang ZH. Accuracy assessment of three-dimensional surface reconstructions of in vivo teeth from cone-beam computed tomography. Chin Med J (Engl) 2016;129(12):1464-70
51. Dong T, Xia L, Cai C, Yuan L, Ye N, Fang B. Accuracy of in vitro mandibular volumetric measurements from CBCT of different voxel sizes with different segmentation threshold settings. BMC Oral Health 2019;19(1):206
52. Jacobs R, Salmon B, Codari M, Hassan B, Bornstein MM. Cone beam computed tomography in implant dentistry: recommendations for clinical use. BMC Oral Health 2018;18(1):88
53. Pauwels R, Faruangsaeng T, Charoenkarn T, Ngonphloy N, Panmekiate S. Effect of exposure parameters and voxel size on bone structure analysis in CBCT. Dentomaxillofac Radiol 2015;44(8):20150078
54. Vandenberghe B, Luchsinger S, Hostens J, Dhoore E, Jacobs R. The influence of exposure parameters on jawbone model accuracy using cone beam CT and multislice CT. Dentomaxillofac Radiol 2012;41(6):466-74
55. Katsumata A, Hirukawa A, Noujeim M, Okumura S, Naitoh M, Fujishita M, et al. Image artifact in dental cone-beam CT. Oral Surg Oral Med Oral Pathol Oral Radiol Endod 2006;101(5):652-57
56. Saati S, Eskandarloo A, Falahi A, Tapak L, Hekmat B. Evaluation of the efficacy of the metal artifact reduction algorithm in the detection of a vertical root fracture in endodontically treated teeth in cone-beam computed tomography images: an in vitro study. Dent Med Probl 2019;56(4):357-63
57. Bezerra IS, Neves FS, Vasconcelos TV, Ambrosano GM, Freitas DQ. Influence of the artefact reduction algorithm of Picasso Trio CBCT system on the diagnosis of vertical root fractures in teeth with metal posts. Dentomaxillofac Radiol 2015;44(6):20140428

How to cite this article: Alrashed S, Dutra V, Chu T-MG, Yang C-C, Lin W-S. Influence of exposure protocol, voxel size, and artifact removal algorithm on the trueness of segmentation utilizing an artificial-intelligence-based system. J Prosthodont. 2024;33:574–83. https://doi.org/10.1111/jopr.13827